Heavy and Complex X-ray Absorption Towards the Nucleus of Markarian 6

J. J. Feldmeier and W. N. Brandt
Department of Astronomy and Astrophysics, Penn State University, 525 Davey Lab, University Park, PA 16802

M. Elvis
Harvard-Smithsonian Center for Astrophysics, 60 Garden Street, Cambridge, MA 02138

A. C. Fabian and K. Iwasawa
Institute of Astronomy, Madingley Road, Cambridge CB3 0HA U.K.

and

S. Mathur
Harvard-Smithsonian Center for Astrophysics, 60 Garden Street, Cambridge, MA 02138

ABSTRACT

We have used the *ASCA* satellite to make the first X-ray spectra of Markarian 6, a bright Seyfert 1.5 galaxy with complex and variable permitted lines, an ionization cone, and remarkable radio structures. Our 0.6–9.5 keV spectra penetrate to the black hole core of this Seyfert and reveal heavy and complex intrinsic X-ray absorption. Both total covering and single partial covering models fail to acceptably fit the observed absorption, and double partial covering or partial covering plus warm absorption appears to be required. The double partial covering model provides the best statistical fit to the data, and we measure large column densities of $\approx (3–20)\times 10^{22}$ cm^{-2} irrespective of the particular spectral model under consideration. These X-ray columns are over an order of magnitude larger than expected based on observations at longer wavelengths. Our data suggest that most of the X-ray absorption occurs either in gas that has a relatively small amount of dust or in gas that is located within the Broad Line Region. The X-ray absorber may well be the putative 'atmosphere' above the torus that collimates the ionization cone. We also detect an apparently broad 6.4 keV iron Kα line, and we present optical spectra demonstrating that the optical emission lines were in a representative state during our *ASCA* observation.

Subject headings: galaxies: individual (Markarian 6) – galaxies: Seyfert – X-rays: galaxies

1. Introduction

X-ray observations of Seyfert galaxies penetrate into the centermost regions of these vigorous objects and are highly effective at studying gas and dust along the line of sight to the black hole core. The nuclear X-ray source is generally thought to be even more compact than the Broad Line Region (BLR) and hence provides a geometrically simple (when viewed from afar) emission region right at the heart of the Seyfert. X-rays are photoelectrically absorbed by neutral atomic gas and molecular gas in essentially the same manner, and most dust grains absorb X-rays as would an equivalent amount of neutral gas. Highly ionized gas can also be effectively probed by means of oxygen and other X-ray absorption edges. In this paper, we use 0.6–9.5 keV spectra provided by the Japan/USA *Advanced Satellite for Cosmology and Astrophysics* (*ASCA*; see Tanaka, Inoue & Holt 1994) to perform the first detailed study of the X-ray emission and absorption properties of Markarian 6 (IC 450; $V \approx 14.2$, see Weedman 1972; $V_0 = 5784 \pm 10$ km s^{-1}, see Meaburn, Whitehead & Pedlar 1989). We also present results from nearly simultaneous optical spectroscopy. Mrk 6 is an S0 galaxy that contains a Seyfert nucleus of type 1.5 (e.g. Osterbrock & Koski 1976 and references therein). Its optical hydrogen lines have a great deal of structure and have shown substantial profile variations (e.g. Khachikian & Weedman 1971, also see Adams 1972; Rosenblatt et al. 1992; Eracleous & Halpern 1993), suggesting that much of the line emitting gas has a spatially coherent bulk velocity field.

Mrk 6 is one of only three type 1 Seyferts which shows evidence for an 'ionization cone' (Meaburn, Whitehead & Pedlar 1989; Kukula et al. 1996; see Wilson & Tsvetanov 1994 for a review of ionization cones). In the context of simple Seyfert unification models, the presence of an ionization cone in a type 1 Seyfert is somewhat surprising. Seyfert 1s are thought to correspond to the geometry where we view the nucleus directly, and hence our line of sight should lie within the cone itself (we would then see a halo morphology rather than a cone-like one). A possible explanation for the presence of ionization cones in some Seyfert 1s postulates that the obscuring torus has a lower density 'atmosphere' (e.g. Evans et al. 1993; Kriss, Tsvetanov & Davidsen 1994; Wilson 1996). Our line of sight skims the surface of the torus and thus passes through the atmosphere. The torus atmosphere is envisaged to have a column density of neutral/low-ionization material of $\approx 10^{20}$–10^{21} cm^{-2}. Such a column is sufficient to be optically thick at all wavelengths between the Lyman edge and soft X-rays (the frequency range of the ionizing radiation), but it allows optical emission from the BLR to pass through with only moderate extinction. Thus we still see a type 1 optical spectrum despite the fact that our line of sight lies outside the ionization cone. *ASCA* observations of the two other type 1 Seyferts with ionization cones, NGC 4151 and Mrk 766 (Weaver et al. 1994; Yaqoob et al. 1995; Leighly et al. 1996), show that they both have complex low-energy X-ray absorption which could arise in torus atmospheres.

Like Mrk 6, both NGC 4151 and Mrk 766 are Seyfert 1.5s (see Osterbrock & Koski 1976 and Osterbrock & Martel 1993), and all three objects may have their AGN aligned in a fairly edge-on manner (e.g. section 3.2 of Evans et al. 1993). A fairly edge-on orientation of the AGN in Mrk 6 is further supported by the length and structure of its impressive radio jet (see Kukula et al. 1996). The large angular size of the Mrk 6 jet when compared to jets seen in other similar type 1 Seyferts suggests that it does not suffer from significant foreshortening by projection effects (consistent with an edge-on orientation).

Absorption in the nucleus of Mrk 6 has been studied at radio, near-infrared and optical wavelengths. In the radio band (see Gallimore et al. 1998 and references therein), H I (21 cm) absorption is detected only towards a bright, compact radio feature located, in projection, $\approx$ 380 pc ($1''$) north of the optical nucleus (the column towards this feature is $\sim 2.6 \times 10^{21}$ cm^{-2}). The radio components nearest to the AGN core did not show H I absorption with 3σ column density limits of $N_{\rm H} \lesssim 4 \times 10^{20}$ cm^{-2} ($T_{\rm spin}$ / 100 K) (Δv / 30 km s^{-1}), where $T_{\rm spin}$ is the spin temperature of the ground state and Δv is the FWHM of the absorption line. However, Gallimore et al. (1998) did not detect a clear radio candidate for the AGN core, and thus it is not clear that radio measurements have constrained absorption along the line of sight to the AGN proper. Several near-infrared and optical observations have been performed in attempts to constrain the reddening to the Narrow-Line Region (NLR) and BLR of Mrk 6. Based on [O II] and [S II] line ratios, Malkan & Oke (1983) suggested a NLR $E(B-V)$ of 0.18 ± 0.08 [here we have removed the $E(B-V)$ due to extinction in our Galaxy]. Assuming a 'Galactic' dust-to-gas ratio (Burstein & Heiles 1978), this $E(B-V)$ corresponds to an absorption column density of $\approx (1.0 \pm 0.4) \times 10^{21}$ cm^{-2}. McAlary et al. (1986) describe attempts to determine the BLR $E(B-V)$ but find that many of the standard hydrogen lines appear to suffer from the effects of high-density radiative recombination (which renders their ratios unreliable as reddening indicators). Rix et al. (1990) have performed Paβ spectroscopy for Mrk 6 and argue that use of this line does allow reliable reddening constraints to be placed upon the BLR. They find that the extinction towards the BLR is no more, and is quite probably less, than $A_V = 2$ [corresponding to $E(B-V) = 0.7$ and an absorption column density of $\approx 4 \times 10^{21}$ cm^{-2}]. Intrinsic extinction and optical polarization are often found together in Seyfert galaxies. Berriman (1989) presents polarimetric measurements for Mrk 6 and finds that it does appear to have some intrinsic polarization (at a level of 0.52 ± 0.15%). However, this level of polarization is not outstanding for type 1 Seyfert galaxies (compare with the 67 other Seyfert 1s in Berriman 1989).

Despite its proximity, brightness and fascinating properties at a variety of wavelengths, Mrk 6 has been very poorly studied in the X-ray regime. To our knowledge, the only X-ray detections of Mrk 6 are a possible *Uhuru* detection (as 4U 0638+74; Forman et al.

1978), a probable *HEAO-1* detection (as 1H 0641+741; Grossan 1992), and a secure *ROSAT* All-Sky Survey (RASS) detection (as 1RXS J065209.8+742537; Voges et al. 1996). Although the *HEAO-1* 5 keV flux density (1.32 ± 0.13 μJy) of Mrk 6 was 79% that of the bright and well-known Seyfert 1 galaxy NGC 3783 (see chapter 2 of Grossan 1992), its flux in the *ROSAT* band was low, with a RASS count rate of only 0.062 ± 0.012 count s^{-1} (for comparison, the RASS count rate of NGC 3783 was 1.4 ± 0.1 count s^{-1}). This discrepancy could be explained if the *ROSAT* flux were reduced due to heavy intrinsic absorption of soft X-rays in Mrk 6.

We proposed and performed an *ASCA* observation of Mrk 6 with several goals in mind. First of all, we wanted to define its basic X-ray properties (e.g. 0.6–9.5 keV flux) far better than has been possible to date. In addition, we wanted to quantify the amount and nature of any intrinsic X-ray absorption so that it could be compared with absorption at other wavelengths. We also wanted to search for flux/spectral variability and study iron Kα line emission. Detection and fitting of a relativistic iron Kα line might, for example, allow the inclination of the inner accretion disk to be constrained. This is of particular interest for Mrk 6 since we have independent indications that the AGN is viewed in a fairly edge-on manner (see above). We obtained nearly simultaneous optical spectra to constrain the state of the optical lines during our *ASCA* observation.

We adopt a distance to Mrk 6 of 77 Mpc ($H_0 = 75$ km s^{-1} Mpc^{-1}). The Galactic neutral hydrogen column density towards Mrk 6 is 6.4×10^{20} cm^{-2} (Stark et al. 1992) and has an expected error of $\lesssim 1 \times 10^{20}$ cm^2 (cf. Elvis, Lockman & Fassnacht 1994).

2. X-ray Observations and Data Analysis

2.1. X-ray Observation Details and Data Reduction

Mrk 6 was observed with *ASCA* on 7–8 April 1997 during the AO-5 observing round. Both Solid-state Imaging Spectrometer CCD detectors (SIS0 and SIS1) and both Gas Imaging Spectrometer scintillation proportional counters (GIS2 and GIS3) were operated. The SIS detectors were operated in 1 CCD mode, and the best calibrated SIS chips were used (chip 1 for SIS0 and chip 3 for SIS1). The SIS chip temperatures varied from -60.1 to -61.6 degrees Celsius for the SIS0 detector, and from -59.4 to -61.4 degrees Celsius for the SIS1 detector. The lower level discriminator was set to 0.47 keV for the SIS detectors. The GIS were operated in PH mode.

We have used the 'Revision 2' processed data from Goddard Space Flight Center (GSFC) for the X-ray analysis below (see Pier 1997 for a description of Revision 2 processing), and data reduction was performed using FTOOLS and XSELECT. We have used the charge transfer inefficiency (CTI) table released on 11 March 1997 [`sisph2pi_110397.fits`; see Dotani et al. 1995 and section 7.7.1 of the AO-6 *ASCA* Technical Description (AN 97-OSS-02) for discussions of CTI]. We have adopted the GSFC Revision 2 screening criteria. After data screening, the total exposure times are the following: 36.7 ks for SIS0, 36.6 ks for SIS1, 36.0 ks for GIS2 and 36.6 ks for GIS3. We have extracted source photons using a circular region of radius $3\overset{\prime}{.}9$ for SIS0, an elliptical region with semimajor axis $4\overset{\prime}{.}4$ and semiminor axis $3\overset{\prime}{.}3$ for SIS1, and circular regions with radii of $5\overset{\prime}{.}0$ for the GIS. The elliptical region for SIS1 provides the best possible ratio of source to background photons, and it prevents the extraction region from extending past the edge of the CCD chip.

2.2. Variability Analysis

To search for flux variations, we binned the data from each detector into 128 s bins, requiring all such bins to be fully exposed. For comparison to the *ASCA* variability results on Seyfert 1 galaxies presented by Nandra et al. (1997a), we use identical energy bands for our analysis: SIS0 + SIS1 full band (0.5–10 keV), SIS0 + SIS1 soft band (0.5–2 keV), SIS0 + SIS1 hard band (2–10 keV), and GIS2 + GIS3 hard band (2–10 keV). The mean count rates per second for each energy band are: 0.227 (SIS full), 0.049 (SIS soft), 0.178 (SIS hard) and 0.153 (GIS hard). We tested for variability by means of a χ^2 test against the hypothesis that the count rate was constant. The reduced χ^2 values found for each band are consistent with no variability, and any sustained variability has an amplitude of less than $\approx 20\%$. We also calculated the normalized 'excess variance' ($\sigma^2_{\rm RMS}$) as defined by Nandra et al. (1997a). The excess variance results, given in units of 10^{-2} $\sigma^2_{\rm RMS}$ (in order to be directly comparable to the results of Nandra et al. 1997a), are 0.46 ± 0.37 (SIS full), -0.02 ± 0.44 (GIS hard), and 0.71 ± 0.49 (SIS hard) where the error bars are at the 68% confidence level. Since the count rate in the SIS soft band was very small, the excess variance results were unreliable, and therefore we do not report them. The excess variances are compatible with minimal or no variability.

2.3. Spectral Analysis

2.3.1. Preparation of Spectra and Fitting Details

Since there is no strong evidence for variability, we have extracted 0.6–9.5 keV SIS and 1.0–9.5 keV GIS spectra using all of the acceptable exposure time. We have grouped these spectra so that there are a minimum of 15 photons per spectral data point, to allow the use of chi-squared fitting techniques. We have used the SISRMG software to generate our SIS redistribution matrix files (rmf), and we use the GIS rmf from 1995 March 6. We generate our ancillary response files (arf) using the ASCAARF software, and we perform spectral modeling using XSPEC (Version 10; Arnaud 1996). Unless stated otherwise, all errors are quoted at the 90.0% confidence level for one parameter of interest ($\Delta\chi^2 = 2.71$).

We first performed spectral fitting for each of the *ASCA* detectors separately, and we obtained results that were consistent to within the errors. We have therefore jointly fitted the spectra from all four detectors, and we detail these results below. In such joint fitting, we allow the normalization for each detector to be free (to allow for small calibration uncertainties in the absolute normalizations between detectors; this is currently standard practice when performing *ASCA* analysis), but we tie together all other fit parameters across the four *ASCA* detectors. When we quote fluxes and equivalent widths below, we shall quote them for the SIS0 detector.

We adopt 'solar metallicity' and the 'solar photosphere' abundance pattern from Table 2 of Anders & Grevesse (1989) for our fitting of intrinsic absorption models (unless stated otherwise).

2.3.2. Basic Spectral Fitting

In this section, we shall number the various X-ray spectral models as they are introduced. For the main models discussed below, the relevant model parameters are given in Table 1. We compare several of the spectral models discussed below in Figure 1a. We also display the SIS0 residuals for Models 1–7 in Figure 2. These show the systematic trends in the residuals that are not apparent from only the numerical value of χ^2_ν.

We began by fitting the spectra with a power-law plus neutral Galactic absorption model (Model 1). $N_{\rm H}$ was constrained to lie within the radio-determined Galactic column density range of $(5.4–7.4)\times10^{20}$ cm^{-2}. This model gives a reduced χ^2 of 1.33 for 778 degrees of freedom, and hence it is rejected with over 99% confidence according to the P($\chi^2 \mid \nu$) function as defined in section 6.2 of Press et al. (1989). The model left systematic residuals throughout the spectrum, and the fitted power law was extremely flat ($\Gamma = 0.01^{+0.03}_{-0.03}$). Such a flat intrinsic power law is not expected from a Seyfert 1 galaxy. Compilations of intrinsic *ASCA* photon indices for Seyfert 1 galaxies (e.g. Brandt, Mathur & Elvis 1997; Nandra et al. 1997b) show almost none less than 1.6. The flat photon index and systematic residuals could arise as the result of intrinsic absorption that has not been taken into account. Therefore, we next added intrinsic absorption in Mrk 6 itself to the power-law plus Galactic absorption model (Model 2). Although this model did find a large amount of intrinsic absorption in Mrk 6 [$N_{\rm H,Mrk\ 6} = (1.19^{+0.16}_{-0.15}) \times 10^{22}$ cm^{-2}], it is still a poor fit to the data with a reduced χ^2 value of 1.08. For 777 degrees of freedom, it is ruled out at the 94.0% confidence level. The model left obvious positive residuals (i.e. the data points were above the model) at the soft end of the X-ray spectrum, and again the best-fitting power law is flatter than expected for a Seyfert 1 galaxy ($\Gamma = 0.56^{+0.07}_{-0.09}$). If we constrain the power law in Model 2 to have a photon index of at least 1.6 (Model 3), we obtain $N_{\rm H,Mrk\ 6} = (3.66^{+0.17}_{-0.16}) \times 10^{22}$ cm^{-2} and $\chi^2_\nu = 1.54$ for 777 degrees of freedom. Large systematic residuals are present throughout the spectrum (see Figure 3), and the fit is ruled out with over 99% confidence.

We next attempted to fit the spectra with models that have been successful in studies of other similar Seyfert galaxies. In the Seyfert 1.5 galaxy NGC 4151, a potentially similar object (see §1), a successful model is that of leakage through a partially covering absorber (e.g. Weaver et al. 1994). Partial covering is also found to be important more generally in the X-ray spectra of intermediate-type Seyferts (e.g. Forster 1998). We therefore tried a model consisting of a power law, Galactic absorption, and a partially covering absorber at the redshift of Mrk 6 (Model 4). Here and hereafter, we constrain the power-law photon index to be at least 1.6 (see the previous paragraph for justification). Model 4 substantially improved the fit to the data over Model 3 ($\Delta\chi^2 = -357.0$), with a reduced χ^2 of 1.09 for 776 degrees of freedom. However, it still left systematic residuals in the soft and hard portions of the spectrum (see Figure 4) and was ruled out at the 95.1% confidence level.

The partial covering in Model 4 is physically equivalent to two components of X-ray emission: (1) a direct, but attenuated, component (perhaps viewed through the torus atmosphere) and (2) a scattered, unattenuated component. There is no reason *a priori* that the X-ray emission should follow only two light paths. In reality, there could be multiple attenuated lines of sight due to, for example, scattering followed by some absorption. In order to better approximate these multiple paths, we fit the data with a model consisting of a power law, Galactic absorption, and two partial covering absorption components (Model 5). The second partial covering component has a much larger column density than the first [$(29.8^{+4.4}_{-9.9}) \times 10^{22}$ cm^{-2} compared to $(3.33^{+0.29}_{-0.16}) \times 10^{22}$ cm^{-2}], but a smaller covering percentage ($55.7^{+5.5}_{-2.9}$% compared to $92.7^{+1.1}_{-0.7}$%). Model 5 provides a substantial improvement in fit quality relative to Model 4 ($\Delta\chi^2 = -128.2$) with the addition of only two more parameters. The model is now a good fit to the data (reduced $\chi^2 = 0.923$), and no large-scale systematic residuals can be seen.

Spectral features due to ionized 'warm' absorption have also been investigated in the X-ray spectra of NGC 4151 and Mrk 766. The strongest features associated with warm absorbers are K-edges from O VII (0.739 keV) and O VIII (0.871 keV), but additional edge and line features are also thought to be present. We have fit the data with a self-consistent photoionized absorber/emitter model constructed from CLOUDY (Ferland 1996) calculations (Model 6; see Reynolds & Fabian 1995 for details of the photoionization calculations). The two free parameters in this model are the ionization parameter ξ and the column density of ionized gas $N_{\rm H,warm}$. We obtain $\xi = 74.1^{+1.6}_{-1.2}$ erg cm s^{-1} and $\log(N_{\rm H,warm}) = 22.95^{+0.02}_{-0.02}$. The model gives $\chi^2_\nu = 1.12$ for 776 degrees of freedom, and hence it is rejected with $> 99\%$ confidence. It is also possible that the spectrum has a combination of partial covering and warm absorption. To test this, we have fit a model consisting of the single partial covering of Model 3 plus the ionized absorption of Model 6 (Model 7; see Table 1 for details). This model provides a statistically acceptable fit to the data.

Out of all the models presented so far, only Models 5 and 7 provide statistically and physically acceptable fits to the data. These models have the same number of degrees of freedom, but Model 5 provides $\Delta\chi^2 = -40.7$ relative to Model 7. Although we cannot rule out the partial covering plus warm absorber model, the double partial covering model is favored by the data, and we have adopted it for further analysis.

We next searched for the presence of the iron Kα fluorescence line. This line has been seen in X-ray spectra of many Seyfert 1 nuclei, and we observe systematic positive residuals at the expected energy (see Figure 4). We added a narrow Gaussian line to Model 5 with a rest-frame energy of 6.4 keV and a fixed width of $\sigma = 20$ eV (Model 8). This model provides an improvement in fit quality of $\Delta\chi^2 = -10.5$ which is significant with over 99% confidence according to the F-test (see tables C-5 and C-6 of Bevington & Robinson 1992). The iron Kα line for Model 8 has an equivalent width of 155^{+92}_{-92} eV. With the presence of the iron Kα line established, we remove our constraint on the line width and allow XSPEC to find the best fitting width (Model 9). The best-fitting intrinsic width for the Gaussian line is 235^{+327}_{-168} eV, suggesting that the line may have some breadth. We find a corresponding equivalent width of 251^{+518}_{-175} eV. We have also experimented with models of a relativistic iron line from the inner part of an accretion disk, but we find the parameters of such models (e.g. orientation) to be poorly constrained due to the limited photon statistics for the line.

2.3.3. Testing of Alternative Continuum Shapes

To examine the robustness of the above results, we have investigated the effects of including additional X-ray continuum components. Our goal is to examine whether a physically-reasonable model with a different X-ray continuum shape can significantly alter our main conclusions.

We began by considering continuum emission from a soft X-ray excess that is made by diffuse hot gas located outside the intrinsic absorber (e.g. Wilson et al. 1992; Weaver et al. 1995). Such gas might be heated by starburst activity in the galactic disk (cf. Baum et al. 1993). To model this gas, we have added a Raymond-Smith thermal plasma (RSTP) component to Models 3, 4, 6 and 7. We have restricted the temperature of the RSTP to be < 1 keV based on X-ray observations of starburst activity in other galaxies, and we allow the metallicity to vary freely. Models 3 and 6 with the RSTP are statistically rejected with over 99% confidence, and Model 4 with the RSTP is not significantly better than Model 4 without it (using the F-test). Model 7 with the RSTP gives a metallicity of 0, and this is unphysical. If we fix the metallicity at solar, we obtain $T \approx 0.9$ keV with $\chi^2 = 734.5$ for 772 degrees of freedom. This is a statistically acceptable fit, although it is not as good as that for Model 5 ($\Delta\chi^2 = 20.2$, and Model 5 has 2 fewer degrees of freedom). In addition, this model still leaves weak systematic residuals above 1 keV.

We then considered soft X-ray excess emission originating from the immediate vicinity of the black hole. We parameterized this soft excess emission in three different ways: blackbody emission, bremsstrahlung emission and RSTP emission. Based on observations of many other Seyfert 1 galaxies, we constrained the temperatures of the soft excess models so that they did not dominate the flux above 1.5 keV. For Model 3, adding soft excess components failed to improve its fit to statistically acceptable levels. The other models tested either did not improve the fit significantly according to the F-test or were not as good as the Model 7+RSTP model of the previous paragraph.

We have also investigated the effects that the Compton reflection continuum might have on our basic absorption results. We started by fitting versions of Model 1 and Model 3 with the simple power law replaced by an exponentially cut-off power law reflected from neutral material (the 'pexrav' model in XSPEC). We constrained the cut-off energy to be > 100 keV and the intrinsic photon index to be in the range 1.6–2.2. Both of these models are statistically rejected (the first at > 99% confidence and the second at > 97.5% confidence) and gave implausibly high reflection fractions (> 10). We then fit a version of Model 4 with the simple power law replaced by the pexrav model. If we do not constrain the reflection fraction, it becomes unphysically large (≈ 9.4). If we constrain the reflection fraction to be < 2, we obtain $\chi^2 = 780.8$ for 774 degrees of freedom. The fit is still not as good as that for Model 5 ($\Delta\chi^2 = 66.5$), and systematic residuals similar to those seen in Figure 4 are still apparent. The reflection fraction 'pegs' at the rather high value of 2, and the statistically best-fitting model is for face-on reflection.

To summarize, inclusion of a soft X-ray excess does not appear to be able to alter our main results regarding the presence of heavy and complex X-ray absorption. While a soft X-ray excess may be present, none of the soft excess models investigated above improves the fit to where it is as good as Model 5. A Compton reflection continuum may also be present, but again it appears to be unable to alter our main absorption results.

2.3.4. Additional Safety and Robustness Checking

We have verified that reasonable deviations from 'solar photosphere' metallicity and abundances do not change our basic absorption results. For example, we have fit a version of Model 3 where we allow both the global metallicity and the individual abundance ratios to vary between 0.2–5 times the solar values (cf. Wheeler, Sneden & Truran 1989). This model can be statistically rejected with $> 99\%$ confidence. Global changes in metallicity with the relative abundances fixed at the solar pattern (from Table 2 of Anders & Grevesse 1989) do not have a large effect on χ^2_ν for all models discussed above. This is because our *ASCA* spectra do not tightly constrain low-energy absorption by H and He, and thus to first order an increase in global metallicity can be offset by a decrease in column density. As a result, the basic line of argumentation in §2.3.2 still applies, and implausibly large metallicities would be needed to resolve the X-ray versus near-infrared/optical absorption discrepancy discussed in §4.2.1.

To further scrutinize our results, we now focus on the power-law photon indices of our models. In all the models where the photon index was constrained to be greater than 1.6, the best-fitting parameters were always found when the index was 'pegged' at the minimum value allowed. As has been stated previously, smaller photon indices are unlikely, yet we would also expect that a physically correct model would not be driven past a hard limit in any reasonable parameter. To investigate this matter, we re-fit Model 5 allowing the photon index to be free. The best-fitting model has a photon index of $\Gamma = 1.46^{+0.23}_{-0.32}$. The best fitting photon index is somewhat smaller than the range observed in Seyfert 1s ($\Gamma \approx$ 1.6–2.2), but it is statistically consistent given the errors. To further examine the limits on the photon index, we re-fit Model 5 fixing the photon index at multiple values throughout the range observed for Seyfert 1s. Although low values of Γ are statistically favored, none of the models could be statistically rejected; the worst fit (for $\Gamma = 2.2$) was rejected at only the 19.3% confidence level. The complex absorption can compensate for steeper intrinsic power laws, and hence the intrinsic photon index is poorly constrained. We stress that steeper power laws only *increase* the amount of absorption required, so the presence of heavy absorption is extremely robust.

Finally, we have repeated our analysis several times using different choices for the CTI table and extraction regions, and none of our main results materially depends upon the details of our specific choices.

2.3.5. Fluxes and Luminosities

We have used our best-fitting model, Model 9, to compute X-ray fluxes and luminosities for Mrk 6. We find an observed 2–10 keV X-ray flux of 1.0×10^{-11} ergs cm^{-2} s^{-1} and an unabsorbed flux of 1.7×10^{-11} ergs cm $^{-2}$ s^{-1}. Due to the strong absorption, the 0.5–2 keV flux found from the model is considerably less: 3.8×10^{-13} ergs cm^{-2} s^{-1} for the absorbed flux and 7.7×10^{-12} ergs cm^{-2} s^{-1} for the unabsorbed flux. Assuming the distance to Mrk 6 stated in §1, the unabsorbed X-ray luminosity is 1.2×10^{43} ergs s^{-1} in the 2–10 keV band and 5.4×10^{42} ergs s^{-1} in the 0.5–2 keV band.

3. Optical Observations and Data Analysis

3.1. Optical Observation Details and Data Reduction

Optical spectra were obtained 33 days before (5 March 1997) and 1 day after (9 April 1997) the *ASCA* observation (see Table 2 for observation details). The spectra were bias-subtracted, flat-fielded and extracted from the CCD frames using IRAF (the APALL task was used for the extraction). The spectra were then wavelength calibrated using He-Ar and Ne lamps for the FAST data and a He-Ne-Ar-Hg-Cd lamp for the MMT data. Finally, the spectra were flux calibrated. The spectrophotometric standard HZ 44 was used to calibrate the FAST observation, and the spectrophotometric standards Hiltner 600 and PG 0823+546 were used for the MMT observation (see Massey et al. 1988 for a discussion of these photometric standards). However, due to poor seeing and slightly non-photometric conditions, we primarily use these calibrations to determine relative fluxes rather than absolute ones. The final reduced spectra for Mrk 6 are shown in Figure 5.

3.2. Optical Analysis and Comparison with Historical Data

Our primary intention in this optical analysis is not to measure flux ratios for all the spectral lines of Mrk 6 (see Koski 1978 and Malkan & Oke 1983 for detailed spectrophotometry), but instead to merely ensure that the variable optical spectrum was in a representative (rather than unusual) state during the *ASCA* observation. This is important for establishing the general applicability of our *ASCA* results; an atypical optical spectrum might suggest that we had observed Mrk 6 during a time when its internal X-ray absorption was unusually high or low. Our second optical observation was only one day after the *ASCA* observation, and there is no historical evidence for strong optical variability on such a short timescale (e.g. Eracleous & Halpern 1993).

To characterize the optical state of Mrk 6, we first used the flux ratio of the broad to narrow components of the Hβ spectral line. This ratio has the advantages of reflecting the nuclear activity of Mrk 6, being well observed historically, and being relatively insensitive to flux calibration uncertainties. Historically, the broad to narrow line ratio has varied from a maximum of 4.5 (see tables 2 and 13 of Rosenblatt et al. 1992) to a minimum of 1.2 (see section III of McAlary et al. 1986). To obtain the narrow line flux for our spectra, we de-blended it from the broad component, assuming that the narrow line component was fit with a Gaussian profile of fixed width found from the unresolved [O II] λ 3727 spectral line. To find the broad line flux, we integrated over the entire Hβ profile, after subtracting the narrow line component and the [O III] λ 4959 line, which is partially blended with the broad component of Hβ. We measure $\frac{F(H\beta_{\rm broad})}{F(H\beta_{\rm narrow})}$ to be 3.3 ± 0.5 for the 5 March 1997 observation and 3.5 ± 0.9 for the 9 April 1997 observation. The error bars are the 1σ errors from setting the continuum level. The measured ratios are consistent with the historical range of activity and support the idea that Mrk 6 was in a reasonably normal optical state at the time of the *ASCA* observation.

We have also determined approximate values for the Balmer decrement for the sum of the broad and narrow line components, after first deblending the [N II] lines from the Hα emission. We find $\frac{F(H\alpha)}{F(H\beta)} = 6.1 \pm 1.2$ for the 5 March 1997 observation and $\frac{F(H\alpha)}{F(H\beta)} = 5.8 \pm 1.4$ for the 9 April 1997 observation, and the errors on these measurements are dominated by the uncertainties involved in flux calibration. Koski (1978) found $\frac{F(H\alpha)}{F(H\beta)} \approx 7.3$ and Malkan & Oke (1983) found $\frac{F(H\alpha)}{F(H\beta)} \approx 7.2$, so again our spectra appear to be reasonably consistent with the historical range of activity for Mrk 6.

Finally, we convolved our spectra with a Johnson V band filter response curve (Bessell 1990) to find an approximate V magnitude. We find $V = 14.6 \pm 0.5$ for the 5 March 1997 observation and $V = 14.9 \pm 0.5$ for the 9 April 1997 observation, where the large error bars are due to the small size of our spectrograph aperture and the non-photometric conditions. These magnitudes appear to be consistent with the historical range of activity. For comparison, Weedman (1972) found $V = 14.2$.

4. Discussion and Conclusions

The most significant result of this work is the detection of heavy and complex X-ray absorption towards the nucleus of Mrk 6. All of our acceptable models clearly show evidence for this absorption, and its presence appears to be extremely robust. Below we will discuss the interpretation of this X-ray absorption, and we will compare it to absorption seen at other wavelengths.

4.1. Comparisons of X-ray, [O III] λ 5007 and Far-Infrared Fluxes

Has our *ASCA* observation penetrated all the way to the black hole region of Mrk 6, or is this region still blocked by even thicker X-ray absorption that *ASCA* cannot penetrate? We do not observe X-ray flux variations, so we are not able to use the presence of rapid X-ray variability as an argument that we are directly observing the black hole region. However, we can compare the measured X-ray flux to fluxes at other wavelengths to address this issue. For example, Mulchaey et al. (1994) have studied a sample of Seyfert galaxies and discuss fairly strong correlations between the 2–10 keV flux (absorption corrected), the [O III] λ 5007 flux, and the far-infrared flux. Using these correlations, the expected 2–10 keV flux can be predicted from the [O III] λ 5007 and far-infrared fluxes. Since it is believed that the [O III] λ 5007 and far-infrared fluxes are reasonably isotropic properties of Seyferts, a large deficit of observed 2–10 keV flux compared to that predicted might indicate the presence of additional extremely thick absorption that *ASCA* cannot penetrate. In this case, we might be observing X-ray flux that has been scattered around the extremely thick absorption and only suffers somewhat lighter absorption.

Using the [O III] λ 5007 and far-infrared fluxes given for Mrk 6 in Mulchaey et al. (1994) and applying the correlations found therein, we predict 2–10 keV fluxes of $\approx 3 \times 10^{-11}$ erg cm^{-2} s^{-1} from the [O III] λ 5007 flux and $\approx 2 \times 10^{-11}$ erg cm^{-2} s^{-1} from the far-infrared flux. Our absorption-corrected 2–10 keV flux from *ASCA* of 1.7×10^{-11} erg cm^{-2} s^{-1} is in reasonably good agreement with these values. Given the intrinsic scatter of the Mulchaey et al. (1994) correlations and potential variability of the X-ray flux, we find no significant discrepancy between the predicted and observed 2–10 keV fluxes. In addition, we note that Mrk 6 has a complex [O III] λ 5007 morphology due to its ionization cone (e.g. Meaburn, Whitehead & Pedlar 1989), and thus the measured [O III] λ 5007 flux from an optical spectrum can depend upon the position angle of the slit on the sky. We see this effect in our optical spectra at the $\sim 40\%$ level, and it may at least partially explain the [O III] λ 5007 discrepancies noted by McAlary et al. (1986). In summary, the observed X-ray flux is entirely consistent with the idea that we have penetrated all the way to the black hole core of Mrk 6. The probable broad iron Kα line discussed in §2 is further suggestive evidence that we are directly observing the black hole region.

4.2. The Physical Properties and Location of the Absorber

4.2.1. The X-ray Versus Near-Infrared/Optical Absorption Discrepancy

Independent of the details of the spectral model under consideration, the X-ray absorption we observe appears to be about an order of magnitude larger than that expected based on earlier studies at longer wavelengths. Our best model (Model 9) involves double partial covering with column densities of $\approx 3 \times 10^{22}$ cm^{-2} and $\approx 2 \times 10^{23}$ cm^{-2}. Rix et al. (1990) have argued using near-infrared/optical data that the extinction to the BLR is no more, and is quite probably less, than $A_V = 2$ (corresponding to a column density of $\approx 4 \times 10^{21}$ cm^{-2} for a 'Galactic' dust-to-gas ratio; see §1 for details). The discrepancy between X-ray absorption and near-infrared/optical extinction cannot be removed by appealing to the effects that high-density radiative recombination can have on hydrogen lines; correcting for such effects would only decrease the inferred near-infrared/optical extinction and thereby exacerbate the discrepancy. Similar absorption discrepancies have been observed in other Seyferts (e.g. section IV of Maccacaro, Perola & Elvis 1982; section 7.2 of Turner & Pounds 1989; section 4.1 Veilleux, Goodrich & Hill 1997).

The X-ray versus near-infrared/optical absorption discrepancy for Mrk 6 reemphasizes the importance of X-ray column density measurements for studies of absorption in Seyfert galaxies. The best efforts at near-infrared and optical wavelengths appear to have failed to expose *most* of the material along the line of sight to the black hole in Mrk 6. To resolve the absorption discrepancy, one is forced to conclude that (1) most of the absorbing material lies within the BLR where it could not be detected by earlier observations and/or (2) the X-ray absorption arises in relatively dust-free gas which causes X-ray photoelectric absorption but not optical extinction (see Maccacaro et al. 1982 for further discussion). Note that these two possibilities need not be mutually exclusive; gas lying within the BLR is quite likely to be relatively dust-free. In fact, the most natural location for a large amount of relatively dust-free gas would be within the dust sublimation radius of the central engine (or perhaps somewhat outside of this region if photoionization-driven sputtering is relevant; see section 2 of Krolik 1996). Following section 5.3 of Laor & Draine (1993), the dust sublimation radius should be ~ 25 light days for Mrk 6.

We also comment that even the smallest X-ray column density is $\gtrsim 75$ times larger than that for the radio components nearest to the AGN core (see §1 and Gallimore et al. 1998). Our interpretation here is that the currently available radio data (the best of which have angular resolutions that correspond to ~ 60 pc) simply do not probe the absorption to the centermost regions. Note that there is currently no radio candidate for the central optical continuum source.

4.2.2. The Location of the X-ray Absorber

In the context of the simplest and most popular version of the unified model for Seyfert galaxies, the heavy X-ray absorption we observe from Mrk 6 might be associated with a compact (< 10 pc), obscuring torus. However, before we interpret our data in terms of this model, we first critically examine other possible locations for absorber.

Malkan, Gorjian, & Tam (1998; hereafter MGT98) have proposed an alternative to the standard unified scheme for Seyfert galaxies known as the Galactic Dust Model (GDM). In the GDM, most of the absorption seen in Seyfert galaxies does not arise within a compact region but is rather due to large-scale (> 100 pc) dust lanes that have little or no physical connection with the central engine. Dust lanes are observed in *Hubble Space Telescope* images of some Seyfert galaxies, and MGT98 find an 'irregular dust' distribution for Mrk 6. However, our data suggest that the GDM is probably not applicable for the bulk of the observed X-ray absorption in Mrk 6. The evidence for X-ray absorption by relatively dust-free gas suggests that the absorber is probably close to the central engine where dust can be sublimated and/or sputtered (see above). In addition, the absorption we see is of the partial covering (rather than the total covering) type, and we have suggested that this is due to the combination of a direct, obscured line of sight and a scattered, unobscured line of sight. It would be somewhat of a geometrical challenge to arrange partial covering absorption by a large-scale dust lane located hundreds of parsecs from the X-ray source. One would need both a fortuitous alignment of small-scale structure in a dust lane as well as an unusually small dust-to-gas ratio (or perhaps unusual dust that only causes grey extinction) for the GDM to be applicable in this particular case.

4.2.3. X-ray Absorption in the Torus Atmosphere?

As discussed in §1, the presence of an ionization cone in Mrk 6 has been used to suggest that we are viewing the nuclear region through a torus 'atmosphere' that blocks most ionizing radiation but lets optical radiation pass through with only moderate extinction. The X-ray absorption we detect appears to be in general agreement with this picture (see Figure 6), and the lack of high optical polarization (see §1) could also result at least partially from this differential absorption as a function of wavelength (in addition, we note that there is probably significant dilution of any polarized optical light by emission from the host galaxy; see Rosenblatt et al. 1992). However, the X-ray column densities we measure are substantially larger than the $\approx 10^{20}$–10^{21} cm^{-2} that have been typically associated with torus atmospheres (see section 7 of Wilson 1996). It appears that we are either detecting an additional absorber located inside the torus atmosphere or that the torus atmosphere is composed of relatively dust-free gas. In the second case, such gas could arise if dust were sublimated in the process of being evaporated off the torus.

The two other Seyfert 1s with ionization cones, NGC 4151 and Mrk 766, also show complex X-ray absorption. Of these two objects, Mrk 6 more closely resembles NGC 4151 in its overall absorption properties. Mrk 766 appears to have a significantly lower neutral column density and is a bright soft X-ray source (see Leighly et al. 1996 and references therein). Mrk 6 and NGC 4151 may be viewed at somewhat larger inclination angles so that our line of sight intercepts thicker and less highly ionized material. Since both NGC 4151 and Mrk 766 show strong X-ray spectral variability, we suspect that Mrk 6 may also show such variability. Systematic monitoring of X-ray spectral variability should give further clues about processes in the torus atmosphere of Mrk 6.

4.2.4. Implications for Other Wavelengths

If the X-ray absorption is indeed due to a torus atmosphere, there are a number of implications for other observations of Mrk 6. Given the X-ray column densities we measure, it is likely that significant free-free absorption will be present at centimeter wavelengths. Applying the relations of Maloney (1996) for the free-free opacity of a torus, we find that the optical depth at 21 cm due to free-free absorption is plausibly of order $\tau_{\rm ff} \sim 5$–100. This large opacity could naturally explain the non-detection of radio continuum emission from the nucleus by Gallimore et al. (1998) and the corresponding non-detection of H I absorption.

The torus atmosphere may also emit coronal lines in the near-infrared and optical, and coronal lines (e.g. [Fe VII] λ 6087) have already been observed from Mrk 6 (Koski 1978). Pier & Voit (1995) hypothesized that much of the coronal line emission from Seyferts comes from a layer just above the surface of the molecular torus, although not all of the coronal line emission need come from this region (see Murayama & Taniguchi 1998). High-resolution spectroscopic observations of optical coronal lines such as [Fe VII] λ 6087 and [Fe X] λ 6375 may allow a probe of the dynamics of the torus atmosphere. Near-infrared coronal lines could also provide constraints on its dust content. Ferguson, Korista & Ferland (1997) have calculated the strengths of near-infrared coronal lines over a large range of physical parameters relevant to Seyferts, and they argue that these lines originate in a region of nearly dust-free gas. If large amounts of dust were present in the coronal line region, the near-infrared coronal lines of calcium and iron would be much weaker than generally observed due to shielding of the ionizing radiation and depletion onto dust. Detection of these near-infrared coronal lines from Mrk 6 could thus provide additional evidence for a relatively dust-free torus atmosphere. The near-infrared observations of Mrk 6 to date have either had insufficient resolution, signal-to-noise, or wavelength coverage to search for these coronal lines, but a better study should be possible with current near-infrared detectors.

Finally, if the torus atmosphere is as hot as $\sim 10^5$ K, thermal soft X-ray emission with a luminosity of $\sim 10^{41}$ erg s^{-1} is expected. Our current observations do not place any strong constraints on this emission, and we expect that it will be difficult to separate any such emission from that of a circumnuclear starburst.

4.3. Future X-ray Observations

Based on our results, we identify several future X-ray observations that show particular promise for improving our understanding of Mrk 6. First of all, X-ray spectra at higher energies (e.g. from *RXTE* or *SAX*) would be helpful for measuring the intrinsic continuum shape. Our *ASCA* spectra cannot tightly constrain the slope of the underlying power law due to the heavy and complex absorption, and knowledge of the intrinsic continuum slope would allow even tighter constraints to be placed on the X-ray absorption. Given the variability of the optical line emission and the fact that our line of sight appears to intersect a torus atmosphere, searches for variability of the X-ray absorption properties are also important to perform. Coordinated variability of the X-ray absorption and optical line profiles might be especially revealing. The *XMM*, *Astro-E* and *Constellation-X* missions will allow high-quality spectroscopy of the iron Kα line emission, and it is important to constrain the inner accretion disk inclination by fitting the profile of the apparently broad line (see §1 for further discussion). Finally, *AXAF* imaging would be useful to constrain and/or study any extended soft X-ray emission associated with starburst activity.

5. Acknowledgments

We thank P. Berlind, A. Dobryzcki, J. Huchra and J. Mader for their effort in obtaining the Mrk 6 optical spectra. We thank K. Arnaud, M. Eracleous, K. Forster, K. Mukai and D. Weedman for helpful discussions. We also thank the referee, J. Gallimore, for several useful suggestions. This paper is based upon work supported by NASA grant NAG5-4826. JJF acknowledges support from R. Ciardullo through grant number GO-0612.01-94A from the Space Telescope Science Institute. ACF acknowledges the Royal Society for support, and KI acknowledges the PPARC for support.

REFERENCES

Adams, T. F. 1972, ApJ, 172, L101

Anders, E. & Grevesse, N. 1989, Geochimica et Cosmochimica Acta, 53, 197

Arnaud, K. A. 1996, in Astronomical Data Analysis Software and Systems V: ASP Conference Series 101, ed. Jacoby, G. & Barnes, J. (ASP Press, San Francisco), p. 17

Baum, S. A., O'Dea, C. P., Dallacassa, D., de Bruyn, A. G. & Pedlar, A. 1993, ApJ, 419, 553

Berriman, G. 1989, ApJ, 345, 713

Bessell, M. S. 1990, PASP, 102, 1181

Bevington, P. R. & Robinson, D. K. 1992, Data Reduction and Error Analysis for the Physical Sciences: Second Edition. McGraw Hill, New York

Brandt, W. N., Mathur, S. & Elvis, M. 1997, MNRAS, 285, 25P

Burstein, D. & Heiles, C. 1978, ApJ, 225, 40

Dotani, T., Yamashita, A., Rasmussen, A. & Team, S. 1995, ASCA News, 3, 25

Elvis, M., Lockman, F. J. & Fassnacht, C. 1994, ApJS, 95, 413

Eracleous, M. & Halpern, J. P. 1993, ApJ, 409, 584

Evans, I. N., Tsvetanov, Z., Kriss, G. A., Ford, H. C., Caganoff, S. & Koratkar, A. 1993, ApJ, 417, 82

Fabricant, D., Cheimets, P., Caldwell, N. & Geary, J. 1998, PASP, 110, 79

Ferguson, J.W., Korista, K.T. & Ferland, G.J. 1997, ApJS, 110, 287

Ferland, G.J. 1996, Hazy, a Brief Introduction to Cloudy. University of Kentucky Department of Physics and Astronomy Internal Report

Forman, W., Jones, C., Cominsky, L., Julien, P., Murray S., Peters, G., Tananbaum, H. & Giacconi, R. 1978, ApJS, 38, 357

Forster, K. 1998, PhD Thesis, Columbia University

Gallimore, J. F., Holloway, A. J., Pedlar, A. & Mundell, C. G. 1998, A&A, 333, 13

Grossan, B. A. 1992, PhD thesis, Massachusetts Institute of Technology

Khachikian, E. Y. & Weedman, D. W. 1971, ApJ, 164, L109

Koski, A. T. 1978, ApJ, 223, 56

Kriss, G. A., Tsvetanov, Z. & Davidsen, A. F. 1994, in The First Stromlo Symposium—The Physics of Active Galaxies: ASP Conference Series 54, ed. Bicknell, G. V., Dopita, M. A. & Quinn, P. J. (ASP Press, San Francisco), p. 281

Krolik, J. H. 1996, Vistas in Astronomy, 40 (1), 9 (Proc. of the Oxford Torus Workshop, ed. by M.J. Ward)

Kukula, M. J., Holloway, A. J., Pedlar, A., Meaburn, J., Lopez, J. A., Axon, D. J., Schilizzi, R. T. & Baum, S. A. 1996, MNRAS, 280, 1283

Laor, A. & Draine, B.T. 1993, ApJ, 402, 441

Leighly, K. M., Mushotzky, R. F., Yaqoob, T., Kunieda, H. & Edelson, R. 1996, ApJ, 469, 147

Maccacaro, T., Perola, G. C. & Elvis, M. 1982, ApJ, 257, 47

Malkan, M. A. & Oke, J. B. 1983, ApJ, 265, 92

Malkan, M. A., Gorjian, V. & Tam, R. 1998, ApJS, in press

Maloney, P. 1996, in Cygnus A — Study of a Radio Galaxy, ed. Carilli, C. L. & Harris, D. E. (Cambridge Univ. Press, Cambridge), p. 60

Massey, P. A., Strobel, K., Barnes, J. V. & Anderson, E. 1988, ApJ, 328, 315

McAlary, C. W., Rieke, G. H., Lebofsky, M. J. & Stocke, J. T. 1986, ApJ, 301, 105

Meaburn, J., Whitehead, M. J. & Pedlar, A. 1989, MNRAS, 241, 1P

Mulchaey, J. S., Koratkar, A., Ward, M. J., Wilson, A. S., Whittle, M., Antonucci, R. J., Kinney A. L. & Hurt, T. 1994, ApJ, 436, 586

Murayama, T. & Taniguchi, Y. 1998, ApJ, 497, L9

Nandra, K., George I. M., Mushotzky, R. F., Turner, T. J. & Yaqoob, T. 1997a, ApJ, 476, 70

Nandra, K., George I. M., Mushotzky, R. F., Turner, T. J. & Yaqoob, T. 1997b, ApJ, 477, 602

Osterbrock, D. E. & Koski, A. T. 1976, MNRAS, 176, 61P

Osterbrock, D. E. & Martel A. 1993, ApJ, 414, 552

Pier, E. A. 1997, *ASCA* Getting Started Guide for Revision 2 Data: Version 6.1, NASA/GSFC

Pier, E. A. & Voit, G. M. 1995, ApJ, 450, 628

Press, W. H., Flannery, B. P., Teukolsky, S. A. & Vetterling, W. T. 1989, Numerical Recipes in Pascal. Cambridge University Press, Cambridge

Reynolds, C.S. & Fabian A.C. 1995, MNRAS, 273, 1167

Rix, H., Carleton, N. P., Rieke, G. H. & Rieke, M. 1990, ApJ, 363, 480

Rosenblatt, E. I., Malkan, M. A., Sargent, W. L. W. & Readhead, A. C. S. 1992, ApJS, 81, 59

Schmidt, G. D., Weymann, R. J. & Foltz, C. B. 1989, PASP, 101, 713

Stark, A. A., Gammie, C. F., Wilson, R. W., Bally, J., Linke, R.A., Heiles, C. & Hurwitz, M. 1992, ApJS, 79, 77

Tanaka, Y., Inoue, H. & Holt, S. S. 1994, PASJ, 46, L37

Turner, T. J. & Pounds, K. A. 1989, MNRAS, 240, 833

Veilleux, S., Goodrich, R. W. & Hill, G. J. 1997, ApJ, 477, 631

Voges, W., et al. 1996, IAU Circular, 6420

Weaver, K. A., Yaqoob, T., Holt, S. S., Mushotzky, R. F., Matsuoka, M. & Yamauchi, M. 1994, ApJ, 436, L27

Weaver, K. A., Mushotzky, R. F., Serlemitsos, P. J., Wilson, A. S., Elvis, M. & Briel, U. 1995, ApJ, 442, 597

Weedman, D. W. 1972, ApJ, 171, 5

Wheeler, J. C., Sneden, C. & Truran, J. W. 1989, ARA&A, 27, 279

Wilson, A. S., Elvis, M., Lawrence, A. & Bland-Hawthorn, J. 1992, ApJ, 391, L75

Wilson, A. S. & Tsvetanov Z. I. 1994, AJ, 107, 1227

Wilson, A. S. 1996, Vistas in Astronomy, 40 (1), 63 (Proc. of the Oxford Torus Workshop, ed. by M.J. Ward)

Yaqoob, T., Edelson, R., Weaver, K. A., Warwick, R. S., Mushotzky, R. F., Serlemitsos, P. J. & Holt, S. S. 1995, ApJ, 453, L81

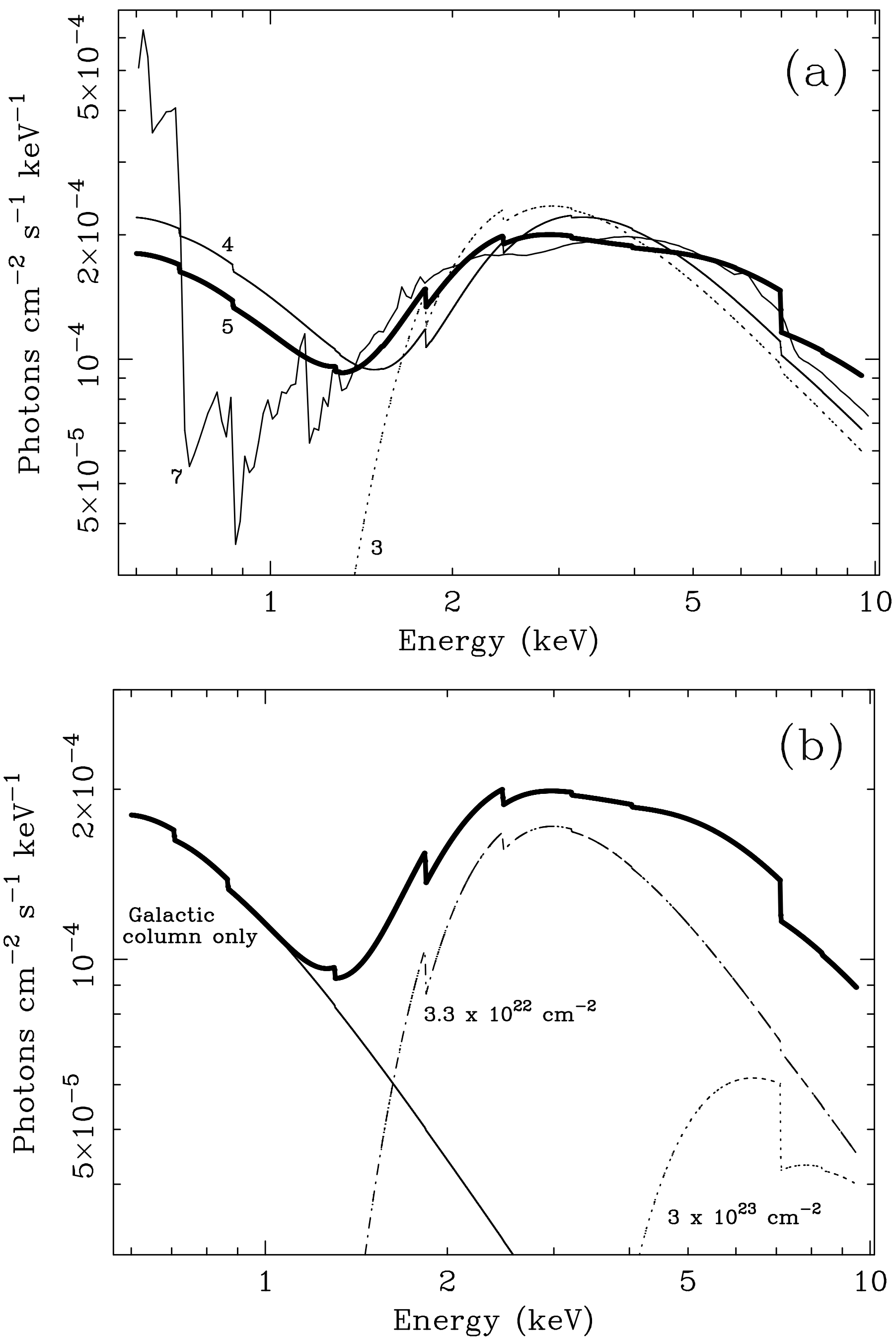

Fig. 1.— (a) Comparison of four of the spectral models fit to the Mrk 6 data (see the text for descriptions of these models). The numbers of the models under comparison are given in the figure itself. The data are fit in the 0.6–9.5 keV band. (b) Decomposition of Model 5 (shown as the thick solid line) into three individual absorbed power laws. Each power law represents one of the lines of sight discussed in §2.3.2. One power law is absorbed by only the Galactic column, one is absorbed by an intrinsic column of $\approx 3.3 \times 10^{22}$ cm^{-2} and one is absorbed by an intrinsic column of $\approx 3 \times 10^{23}$ cm^{-2}.

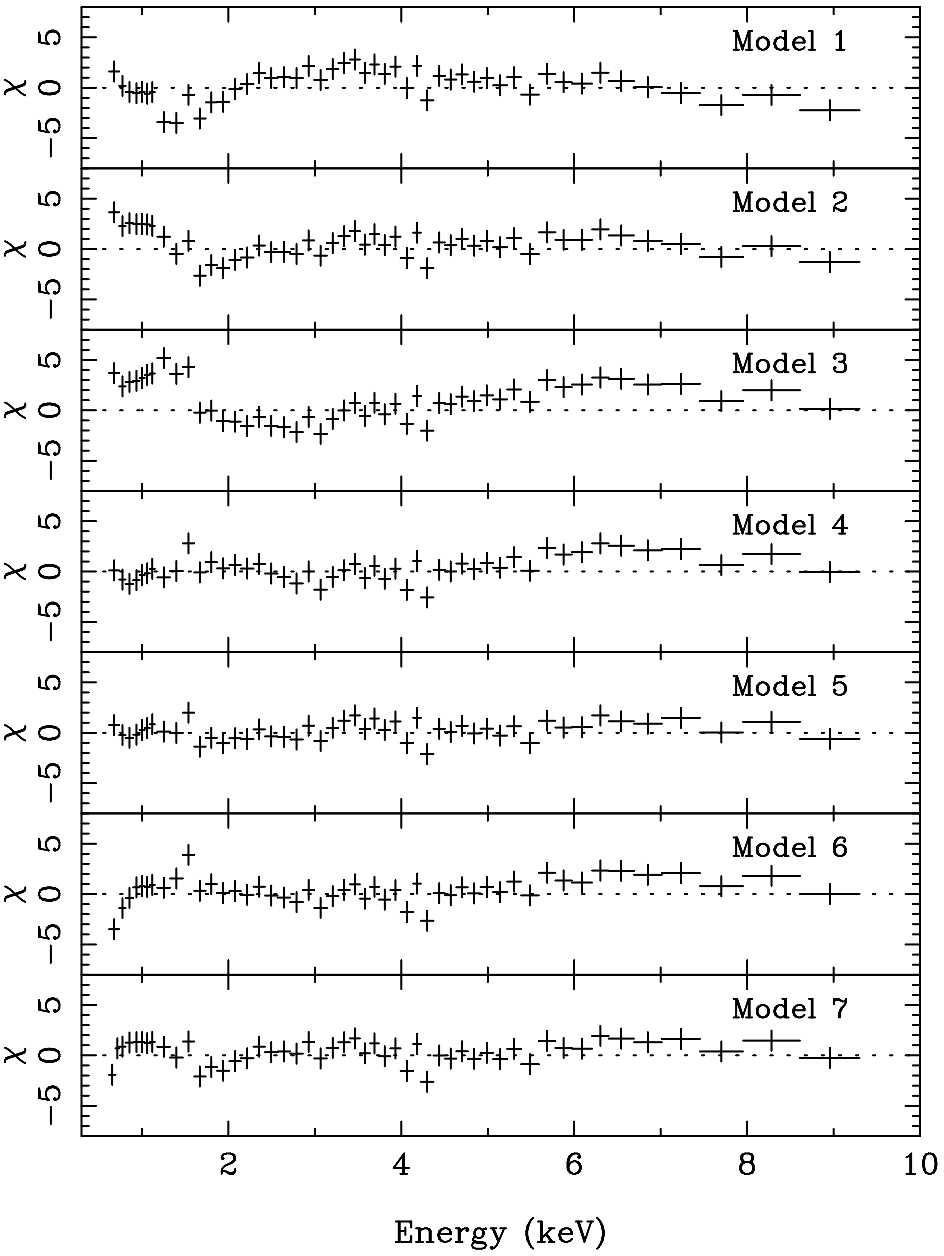

Fig. 2.— *ASCA* SIS0 0.6–9.5 keV fit residuals for Models 1–7 (see the text for descriptions of these models). The ordinates for the panels (labeled χ) show the fit residuals in terms of sigmas with error bars of size one. Only the SIS0 residuals are shown for clarity, but the residuals for all the detectors are in good general agreement.

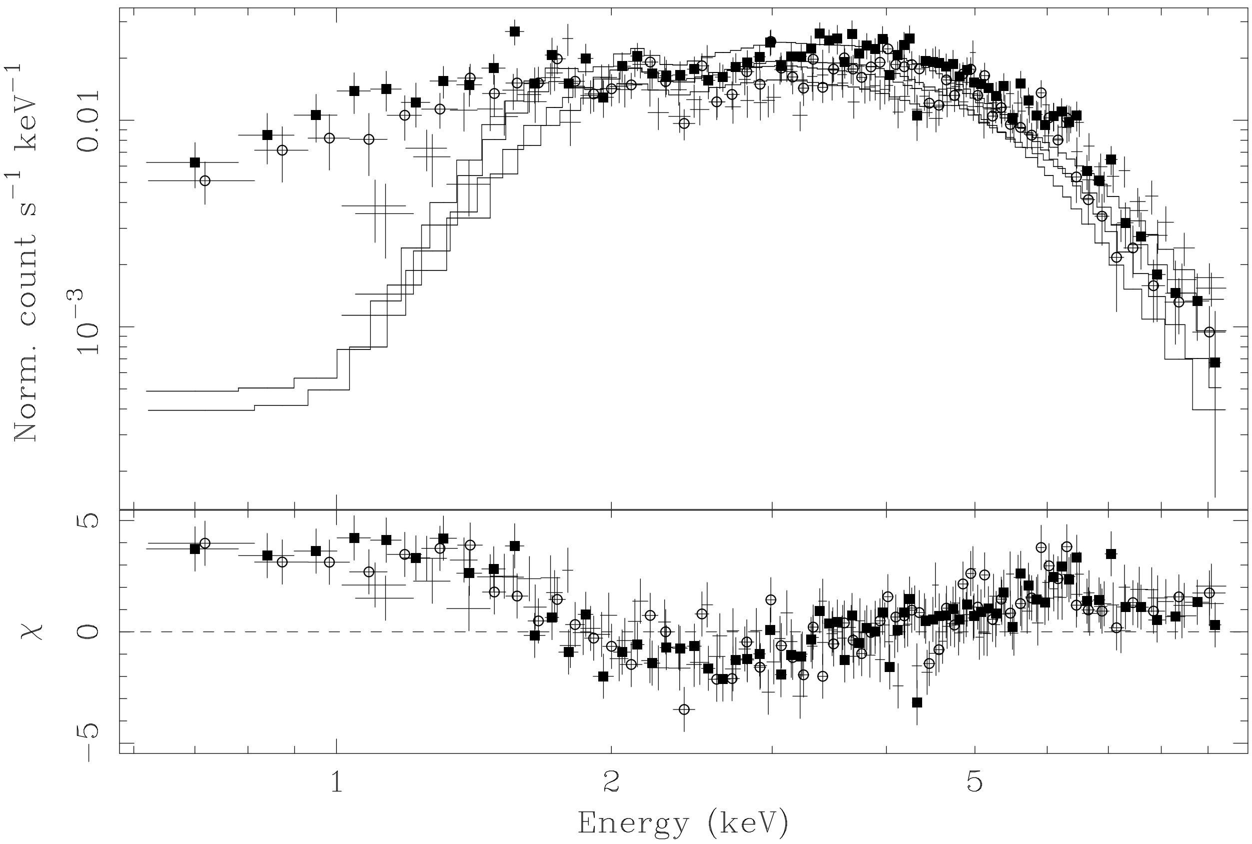

Fig. 3.— *ASCA* SIS0 (solid squares), SIS1 (open circles) and GIS (plain crosses) spectra of Mrk 6 (shown in the observed frame). A model consisting of a power law, Galactic absorption, and intrinsic absorption in Mrk 6 has been fit to the data (Model 3). As described in the text, the power-law photon index is constrained to be ≥ 1.6. The ordinate for the lower panel (labeled χ) shows the fit residuals in terms of sigmas with error bars of size one. Note the clear systematic residuals throughout the spectrum.

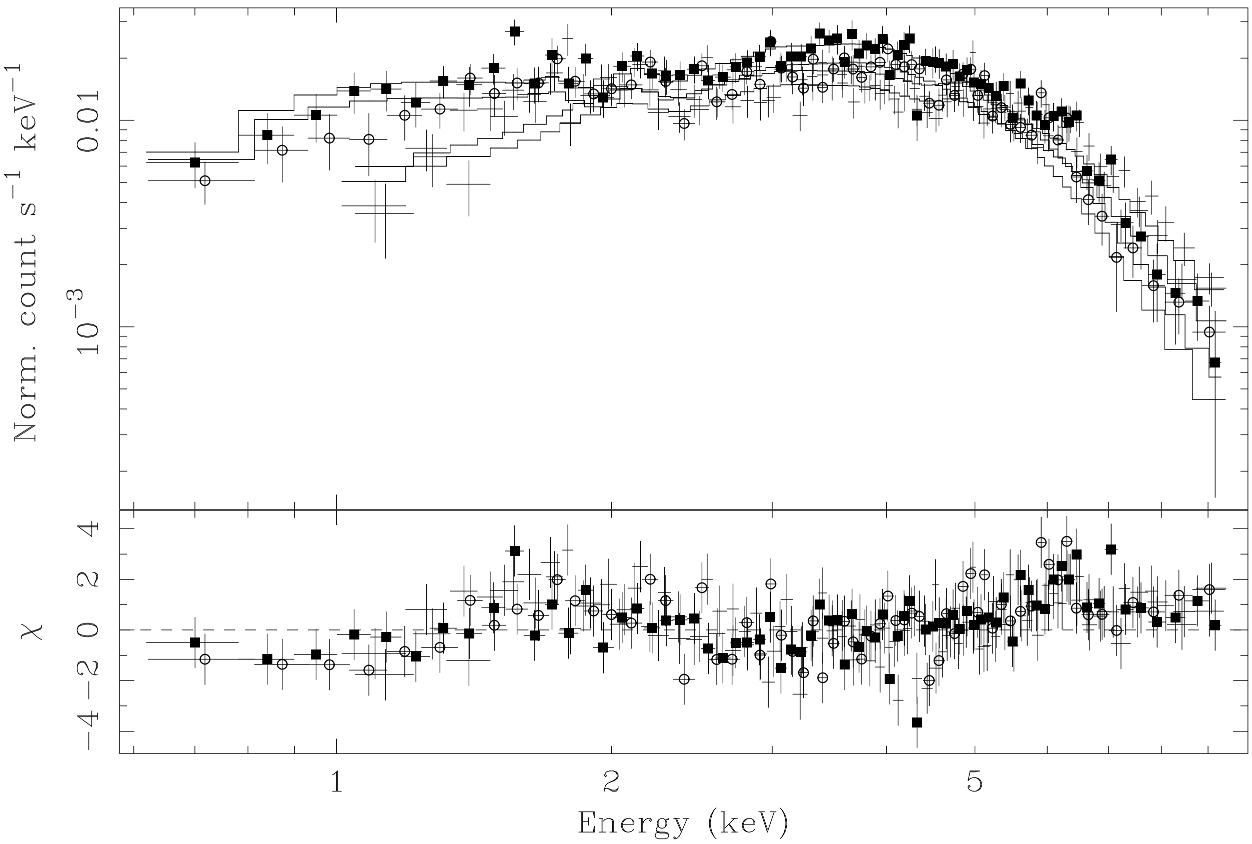

Fig. 4.— *ASCA* SIS0 (solid squares), SIS1 (open circles) and GIS (plain crosses) spectra of Mrk 6 (shown in the observed frame). A model consisting of a power law, Galactic absorption and intrinsic partial covering has been fit to the data (Model 4). The ordinate for the lower panel (labeled χ) shows the fit residuals in terms of sigmas with error bars of size one. Note the 'wave-like' systematic residuals in this model. Also note the systematic positive residuals at the energy of the iron Kα line.

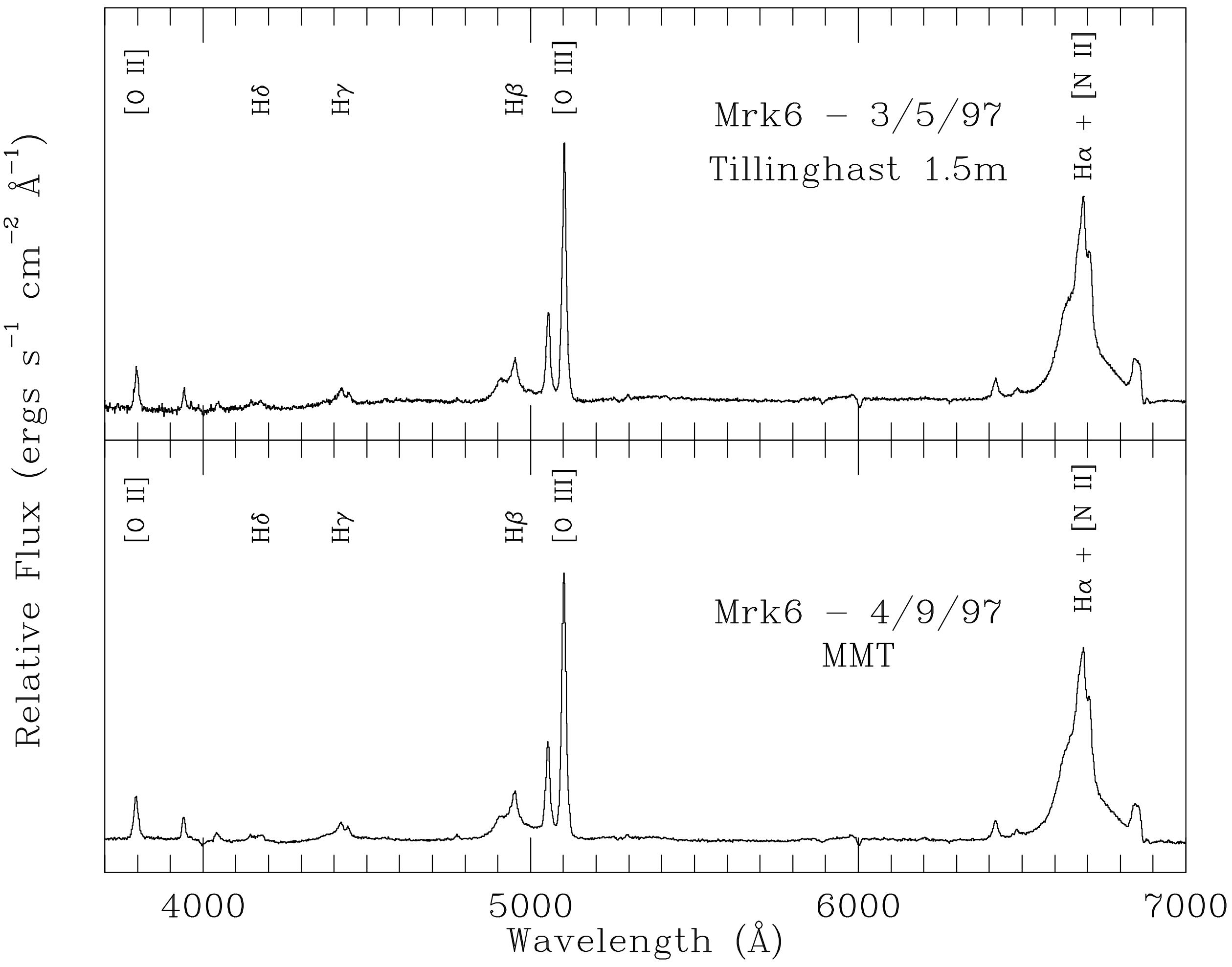

Fig. 5.— Optical spectra of Mrk 6 taken with the Tillinghast 1.5 m and the MMT. The locations of prominent emission lines are shown. Note the broad blue-shifted components of Hβ and Hα, though Hα is also blended with [N II].

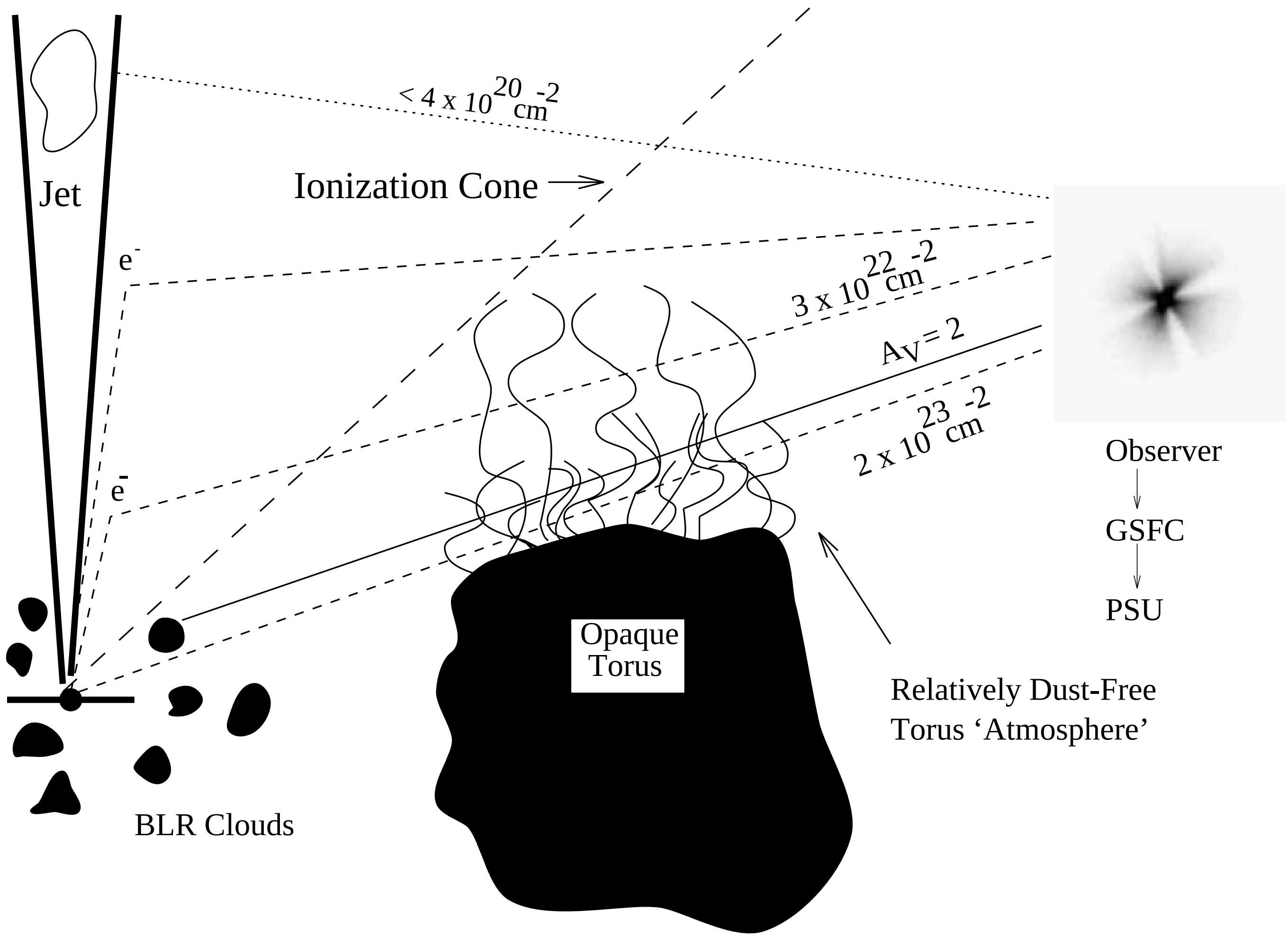

Fig. 6.— Sketch of the absorption geometry in Mrk 6 for Model 9. The short-dashed lines show the X-ray lines of sight, the solid line shows the near-infrared/optical line of sight for one BLR cloud, and the dotted line shows a radio line of sight. The near-infrared, optical and X-ray radiation intercepts a relatively dust-free torus 'atmosphere' that blocks ionizing radiation but allows near-infrared/optical radiation to pass through with only moderate extinction. This torus atmosphere is thereby responsible for collimating the observed ionization cone (one edge of which is shown by the long-dashed line). We list the fitted X-ray absorption column densities next to the corresponding short-dashed lines (see Table 1), and we also show the A_V from Rix et al. (1990) next to the near-infrared/optical line of sight. The strongest radio emission does not originate from the immediate vicinity of the nucleus. The grayscale image at the right hand side shows the *ASCA* SIS image. This sketch is not to scale.

Table 1. *ASCA* Spectral Fitting Results

Parameter Name	PL + GA + ZA 2	PL + GA + PC 4	PL + GA + 2 PC 5	PL + GA + PC + WA 7	PL + GA + 2 PC + Fe 9
	Model Description and Number				
Galactic $N_H/(10^{20}$ cm$^{-2})$	5.4	7.4	7.4	7.4	7.4
Photon Index, Γ	$0.56^{+0.07}_{-0.09}$	1.6 [a]	1.6 [a]	1.6 [a]	1.6 [a]
Redshifted $N_H/(10^{22}$ cm$^{-2})$	$1.19^{+0.16}_{-0.15}$	—	—	—	—
Partial Covering (1) $N_H/(10^{22}$ cm$^{-2})$	—	$4.90^{+0.29}_{-0.27}$	$3.33^{+0.29}_{-0.16}$	$12.3^{+4.2}_{-2.7}$	$3.09^{+0.42}_{-0.79}$
Partial Covering (1) Percentage	—	$93.6^{+0.5}_{-0.5}$	$92.7^{+1.1}_{-0.7}$	$63.4^{+5.1}_{-4.4}$	$92.1^{+1.2}_{-2.1}$
Partial Covering (2) $N_H/(10^{22}$ cm$^{-2})$	—	—	$29.8^{+4.4}_{-9.9}$	—	$18.28^{+3.6}_{-8.7}$
Partial Covering (2) Percentage	—	—	$55.7^{+5.5}_{-2.9}$	—	$50.2^{+9.2}_{-7.2}$
ξ (erg cm s^{-1})	—	—	—	$51.9^{+5.7}_{-4.4}$	—
$\log(N_{\rm H,warm})$	—	—	—	$22.58^{+0.05}_{-0.07}$	—
Line energy	—	—	—	—	6.4 keV (fixed)
Line sigma (eV)	—	—	—	—	235^{+327}_{-168}
Line norm. ($\times 10^{-5}$) [b]	—	—	—	—	$4.6^{+2.5}_{-2.5}$
χ^2 / d.o.f.	839.3 / 777	842.5 / 776	714.3 / 774	755.0 / 774	697.9 / 769
χ^2_ν / P($\chi^2 \mid \nu$)	1.08 / 0.94	1.09 / 0.95	0.923 / 0.06	0.975 / 0.32	0.908 / 0.03

Key: PL = power law, GA = Galactic absorption (constrained to lie within the radio-determined range; see the text), ZA = redshifted absorption, PC = partial covering, WA = warm absorber/emitter model (see the text for details), Fe = iron line. All errors are given at the 90% confidence level for one parameter of interest ($\Delta\chi^2 = 2.71$). P($\chi^2 \mid \nu$) is the chisquared rejection probability as defined in section 6.2 of Press et al. (1989), and larger values of P($\chi^2 \mid \nu$) indicate statistically poorer models.

[a]The photon index was constrained to lie within the range 1.6–2.2. However, in all models, the best-fitting value was found when the photon index was 1.6 (see the text for further discussion).

[b]The line normalization is quoted for the SIS0 detector.

Table 2. Details of Optical Observations

Observation Date	Telescope and Spectrograph [a]	Range (Å)	Dispersion [b] (Å)	Aperture	Exposure Time (s)	P.A.
5 March 1997	Tillinghast 1.5 m — FAST	3650–7500	2.95	$3'' \times 180''$	900	90°
9 April 1997	MMT — Blue Channel	3200–8630	3.92	$2'' \times 150''$	300	−54°

[a]The Tillinghast 1.5 m and Multiple Mirror Telescope (MMT) are located on Mount Hopkins in Arizona. The FAST spectrograph is described in Fabricant et al. (1998), and the Blue Channel spectrograph is described in Schmidt, Weymann, & Foltz (1989).

[b]Dispersion is Å per two pixel resolution element.